

Argon-39 Measurements in the Atlantic and Pacific Oceans

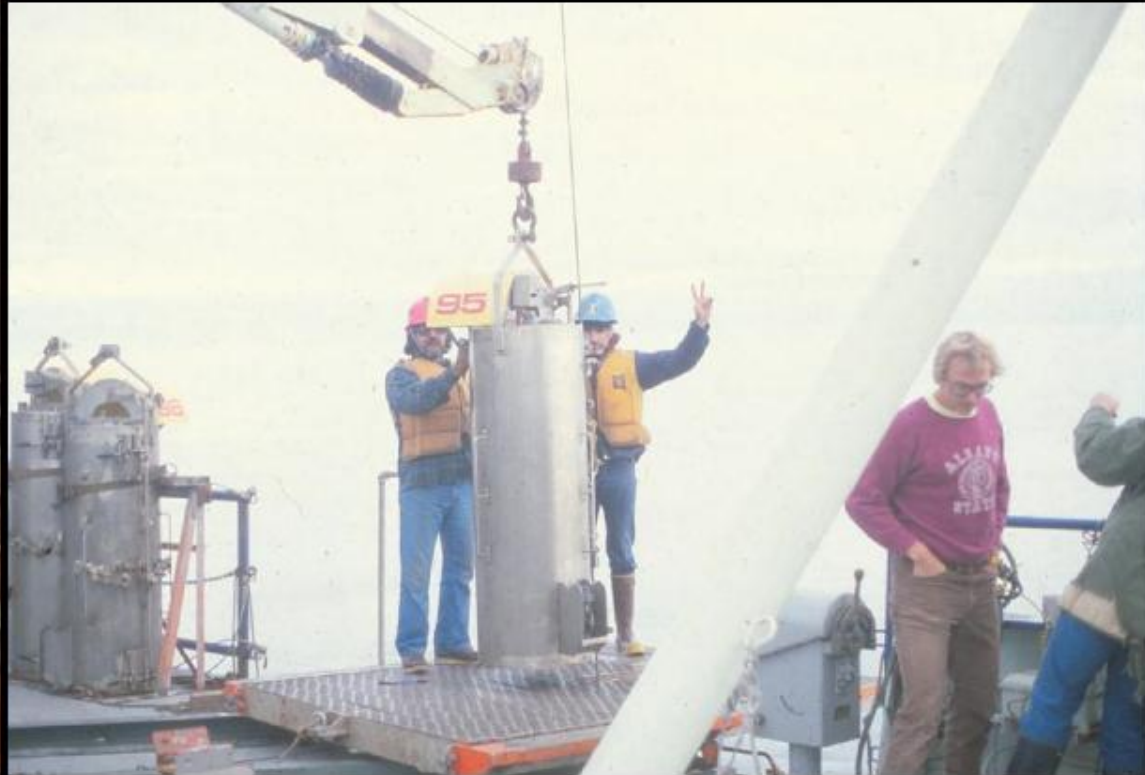
Bill Smethie

Lamont-Doherty Earth Observatory
of Columbia University

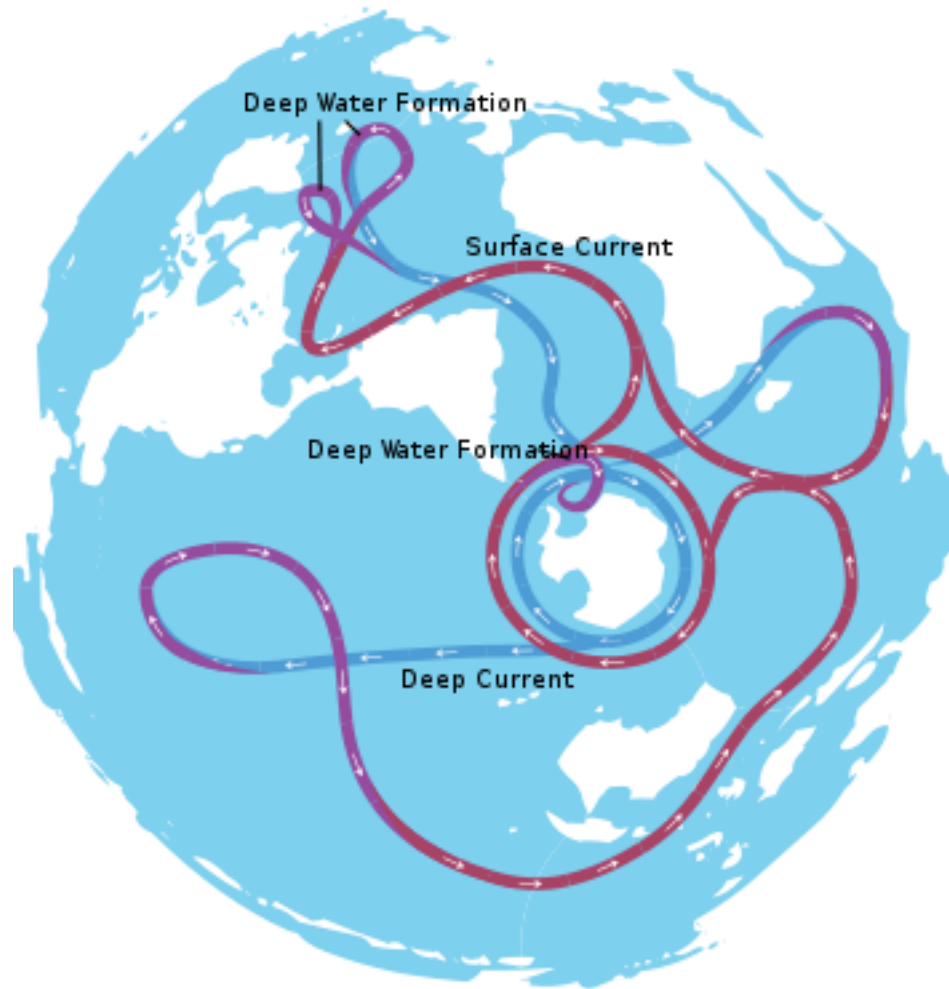
During the 1980s and early 1990s about 125 ocean samples were collected for measurement of Ar-39.

About 75% were collected from the Atlantic Ocean on the TTO and SAVE surveys. Other samples were collected from the Arctic Ocean, the Southern Ocean and the Pacific Ocean. During these programs, C-14 was still being measured by beta counting and 250 liters of water were needed. The TTO program began before CFCs were readily measurable and Kr-85 was one of the suite of tracers funded, which required developing the technology to degas large volumes of water at sea and large volumes were needed for measurement of Ra-228. Large volume samples (250 liters) were obtained using Gerard Barrels. Ar-39 samples were collected by combining 5-6 Gerard Barrels hung over a 50 m depth interval.

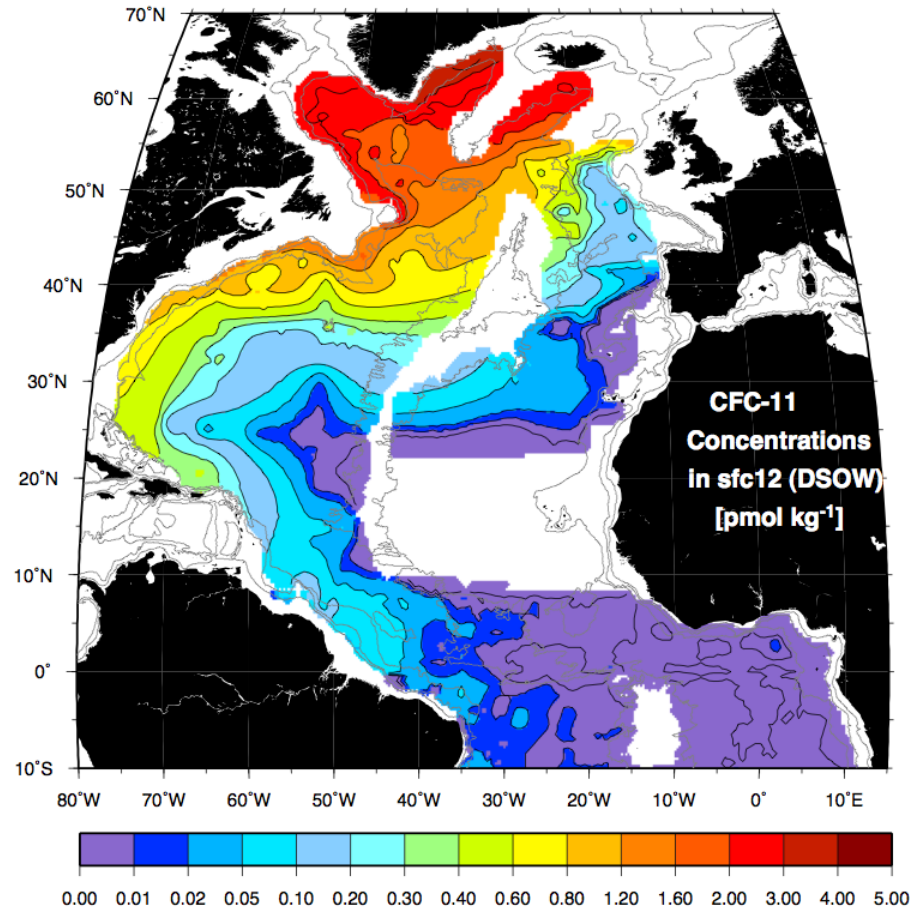
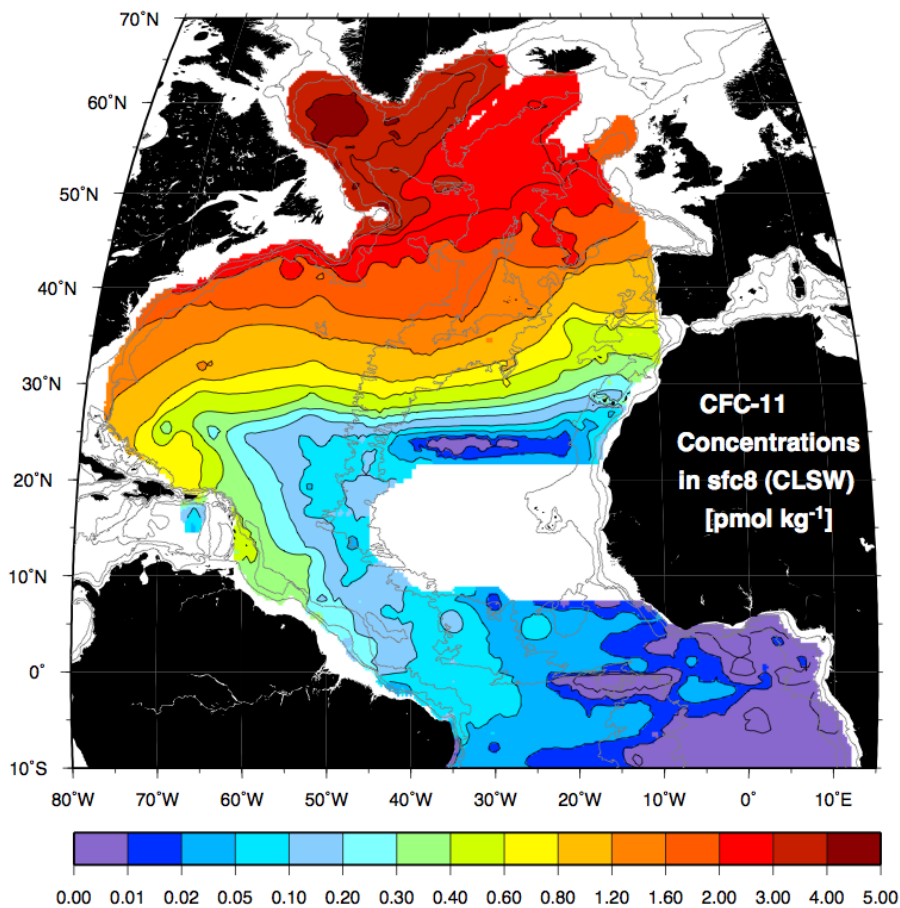
Krypton-85 sampling at sea



Vacuum degassing system (left) and Gerard Barrels (right) use for collecting and degassing water samples for Ar-39 and Kr-85 seawater measurement.

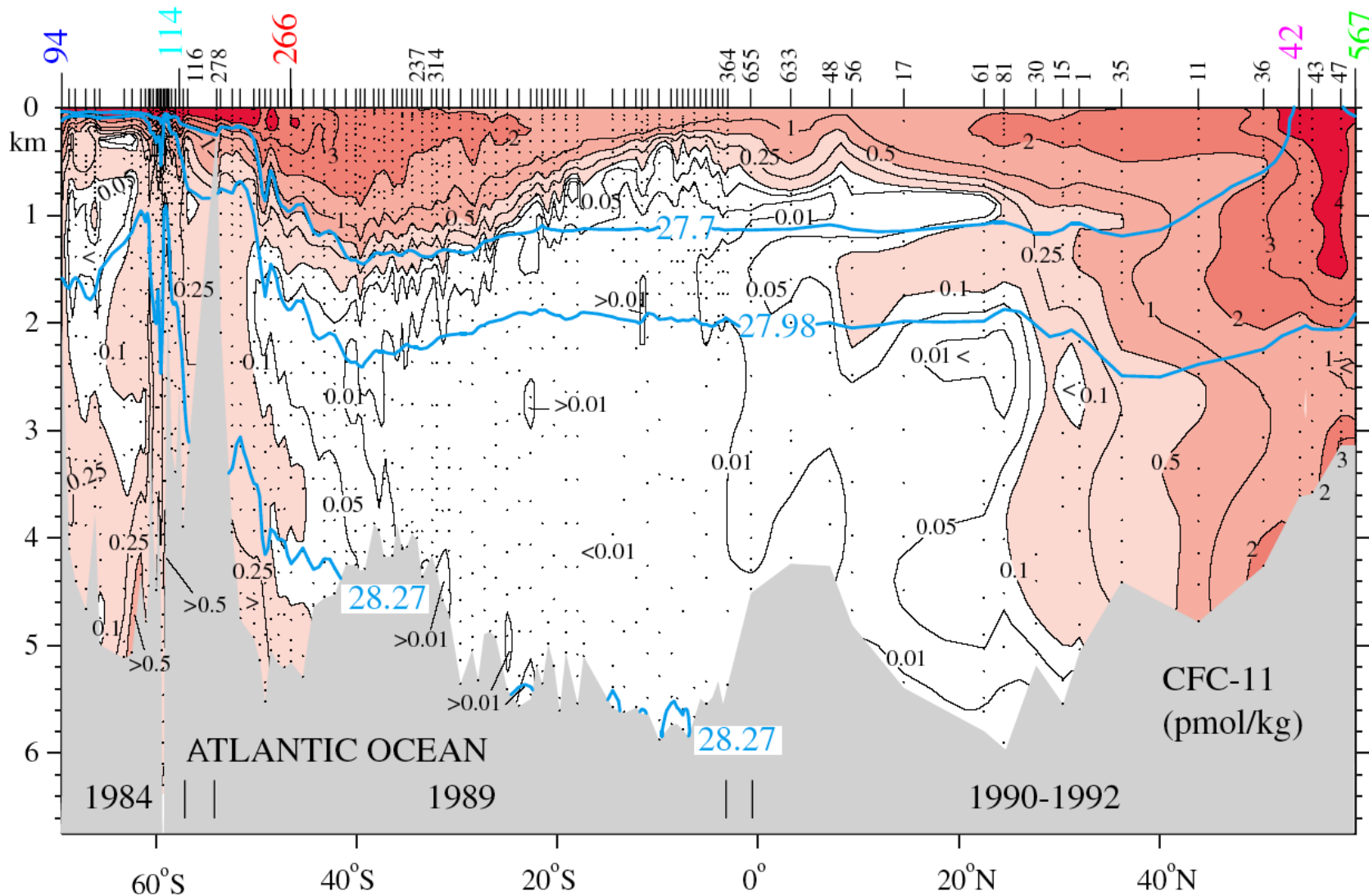


Cartoon of global overturning circulation (Wikipedia)

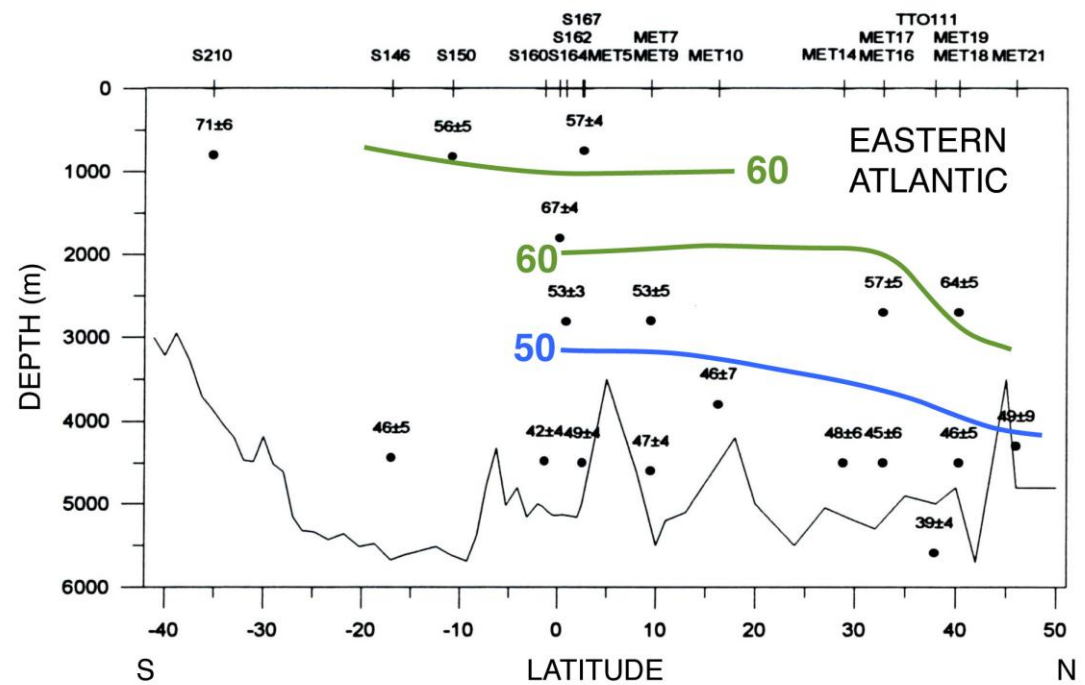
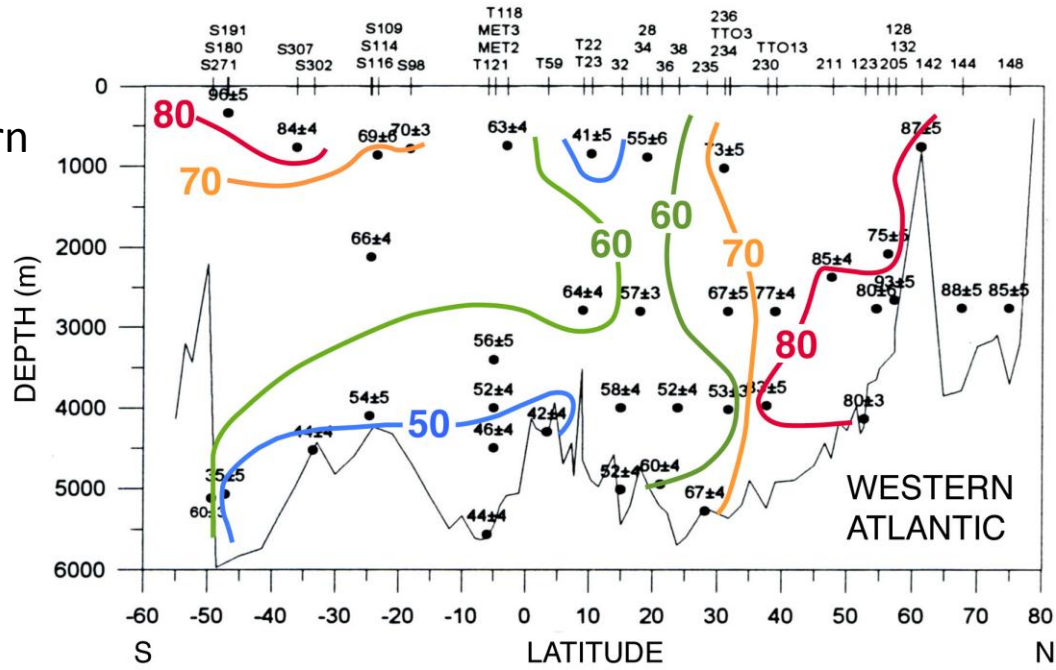


CFC-11 concentration maps for Classical Labrador Sea Water and Denmark Strait Overflow Water based on data collected between 1991 and 1998 (LeBel et al., 2008, Deep-Sea Research 55:891-910)

CFC-11 in the western Atlantic Ocean



Ar-39 (% modern)
sections in the western
and eastern Atlantic
Ocean



Percent Northern Component Water calculated from PO4*

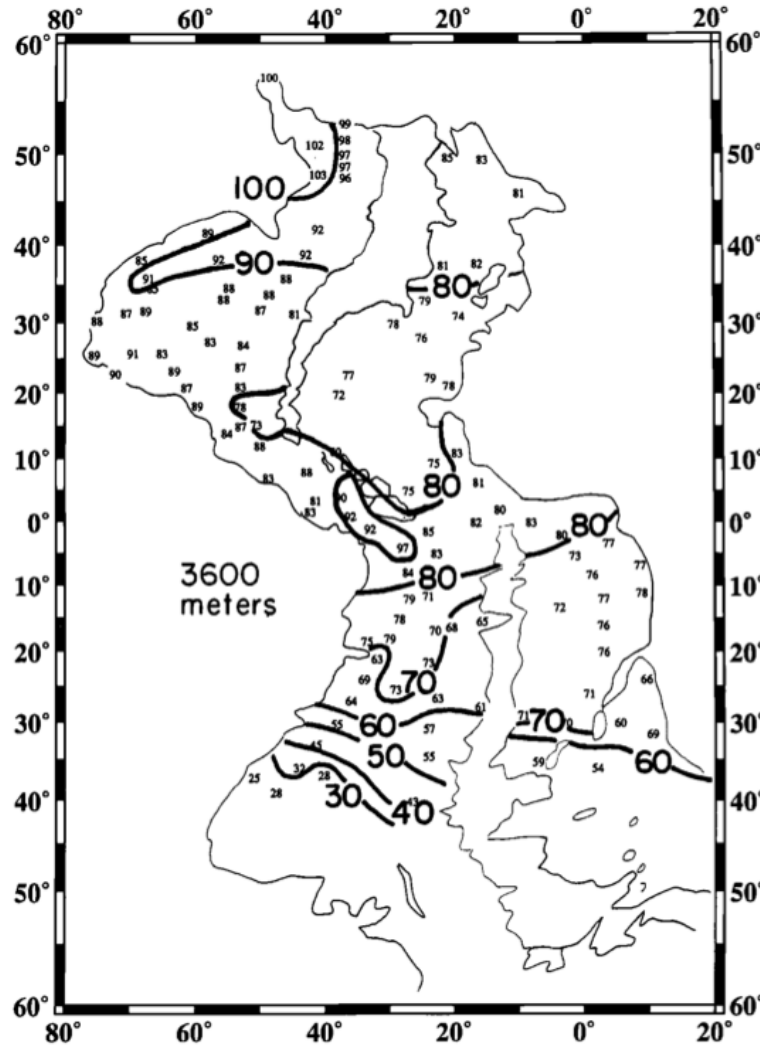


Fig. 5. Map showing percentage of northern component water along the 3600 m depth horizon. The light lines define the geographic boundaries of this horizon.

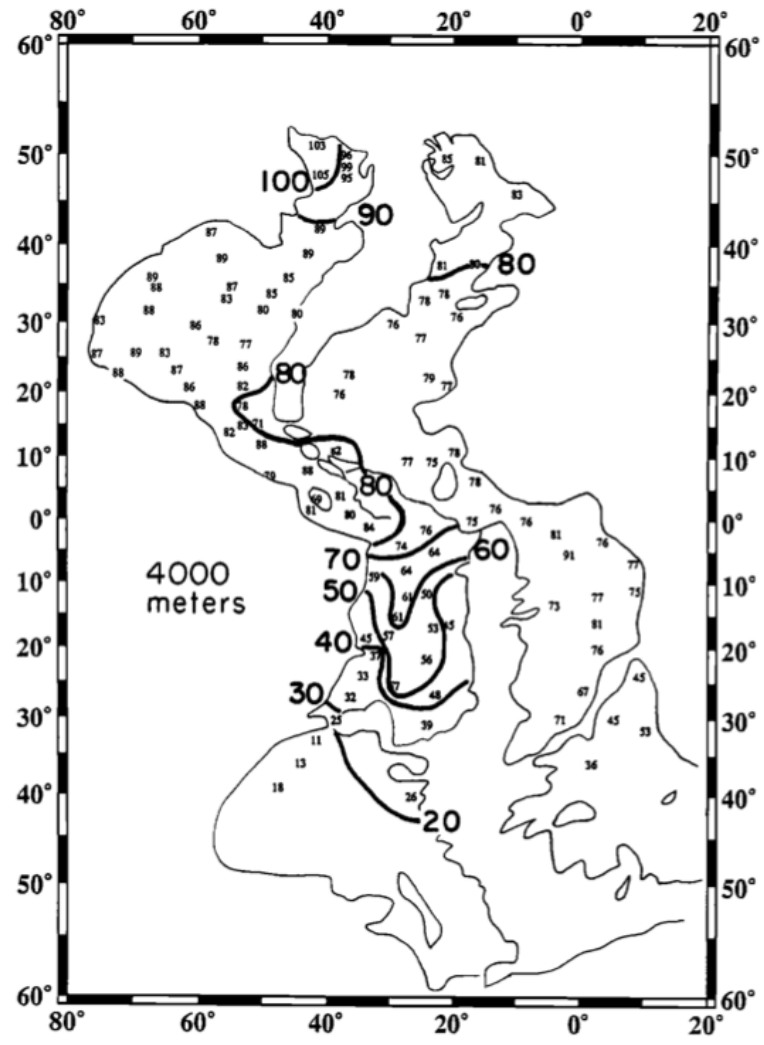
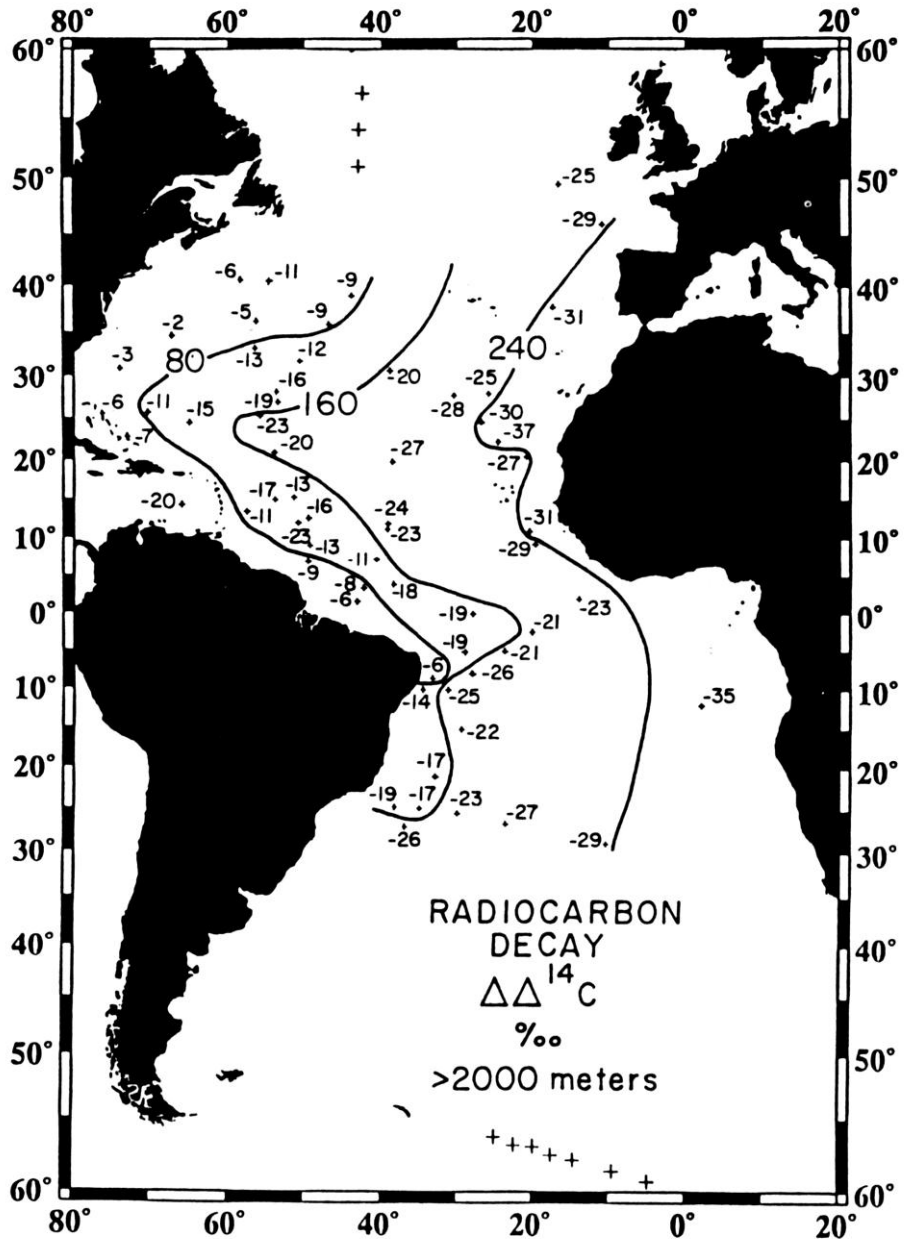
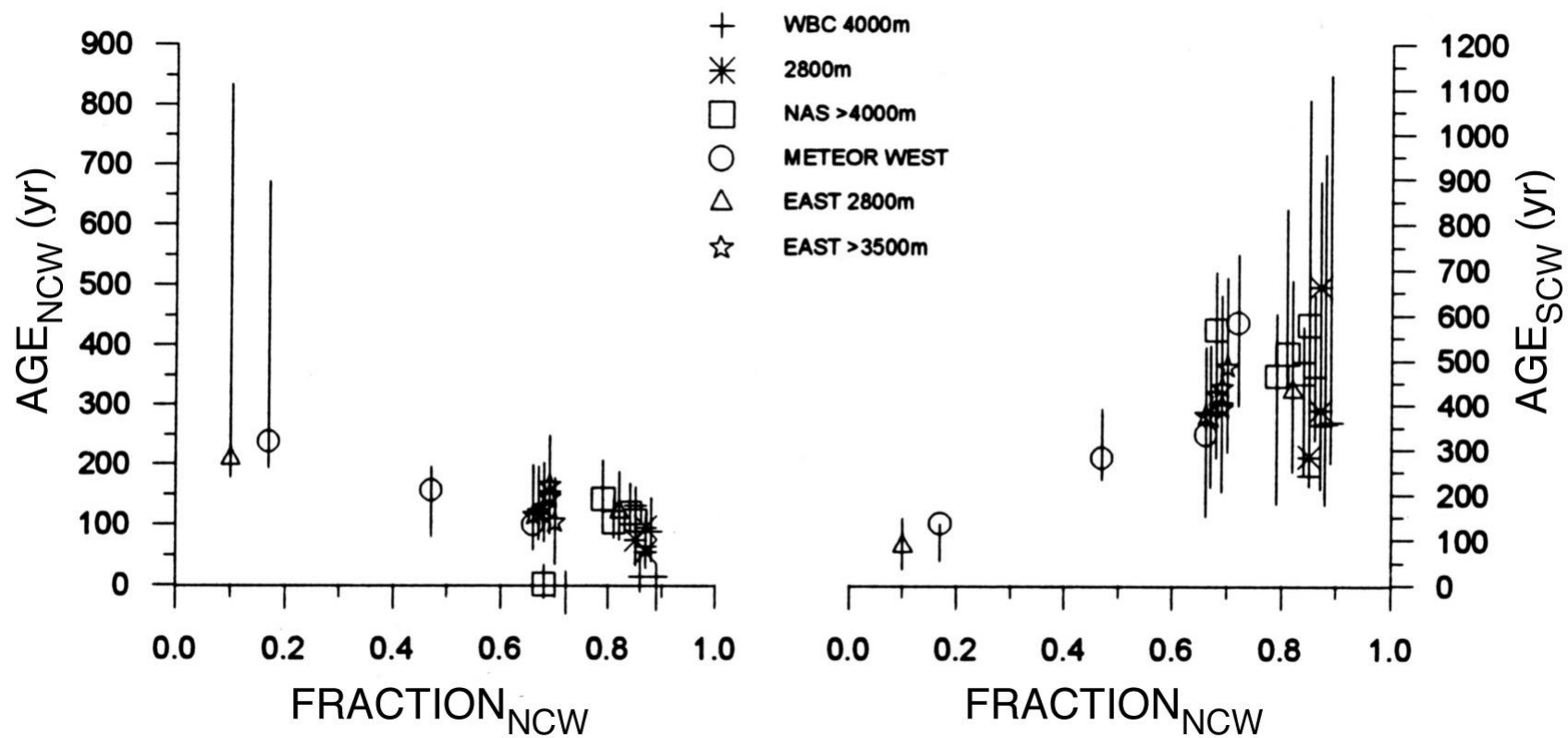


Fig. 6. Map showing fraction of northern component water along the 4000 m depth horizon. The light lines define the geographic boundaries of this horizon.

Radiocarbon Age for Water below 2000 meters

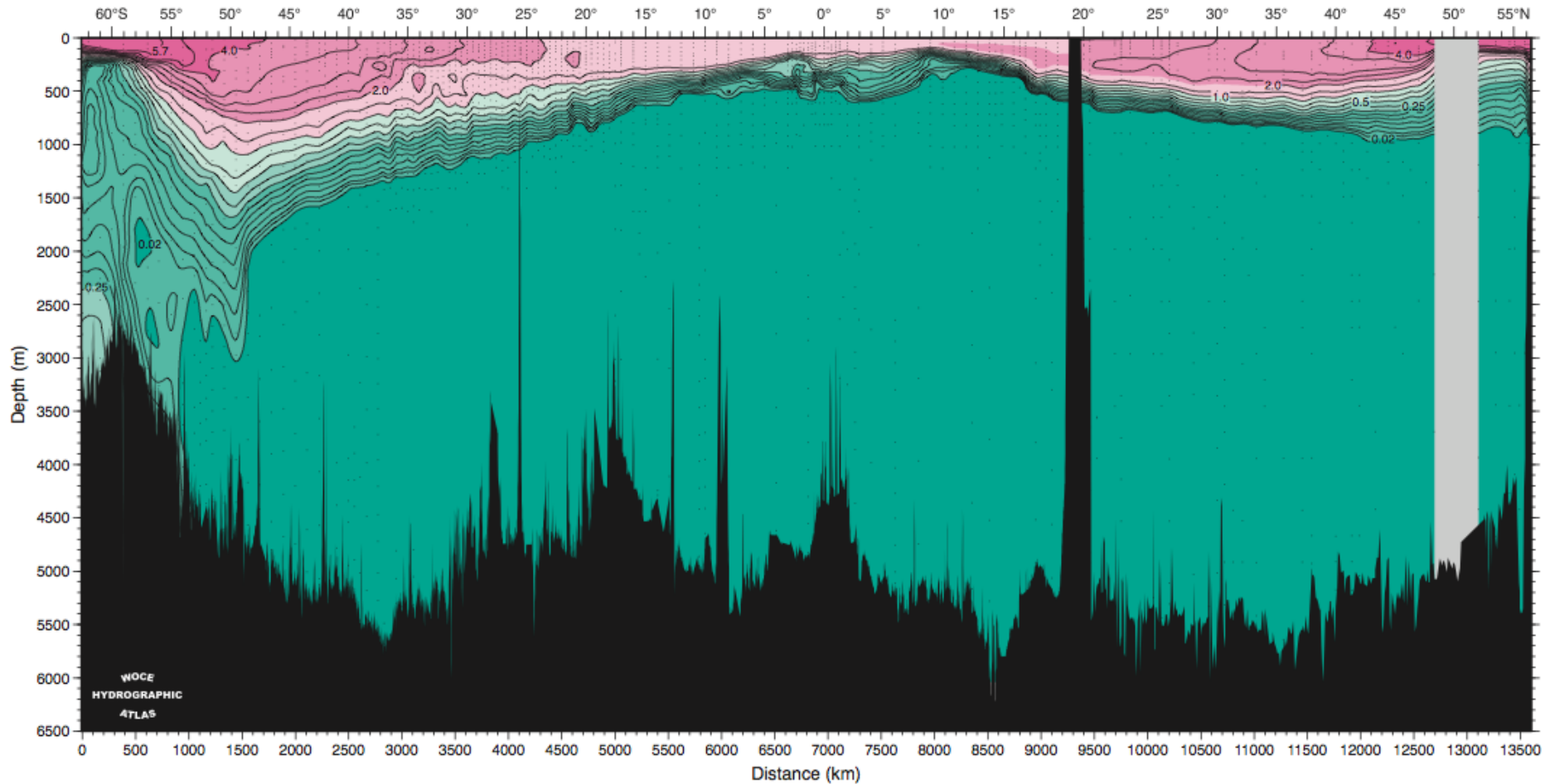


Broecker et al. (1991) Global Biogeochemical Cycles 5:87-117



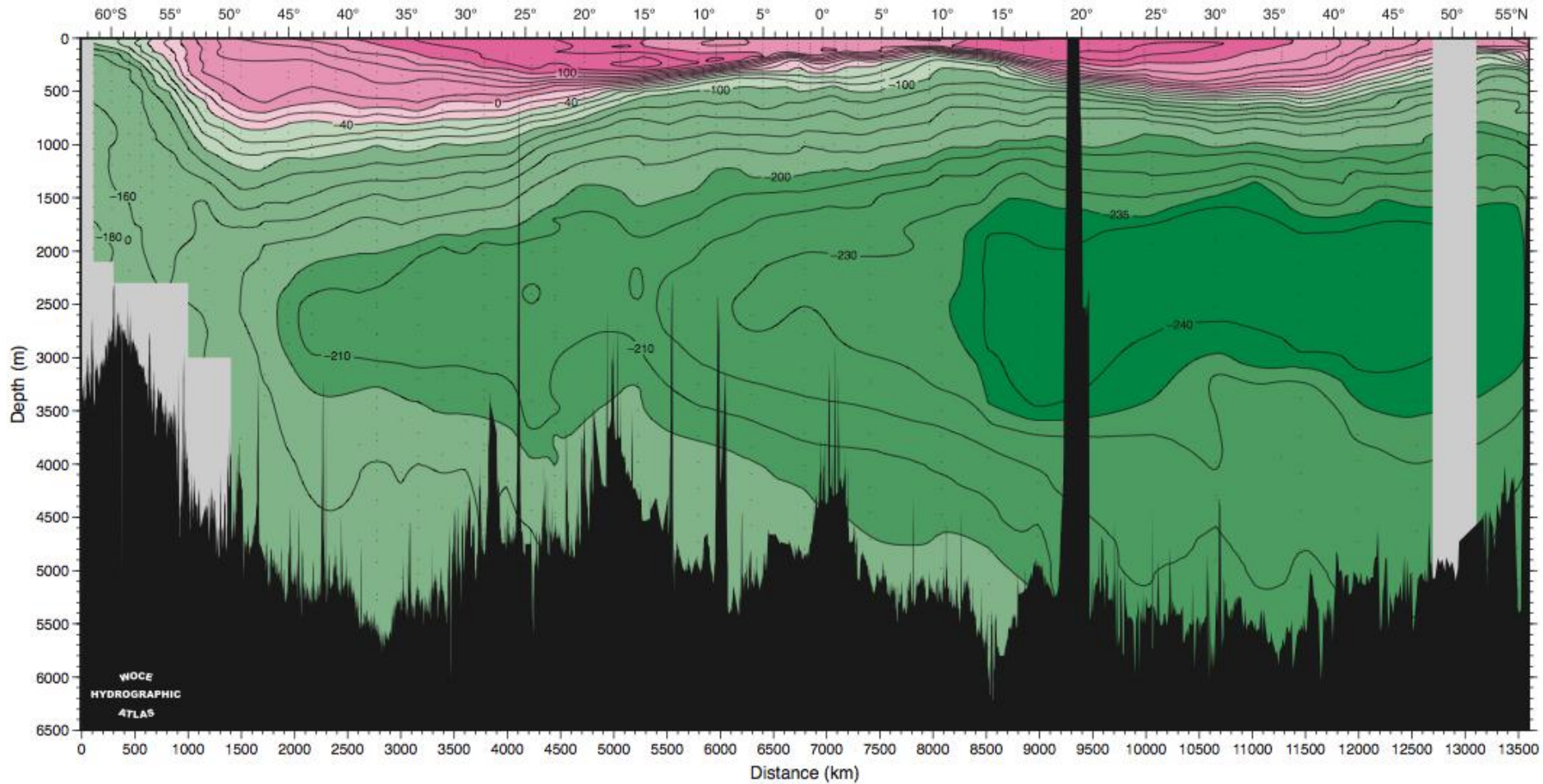
Rodriguez, Ph.D thesis, 1993, University of Bern

CFC-11 (pmol/kg) section in the central Pacific Ocean

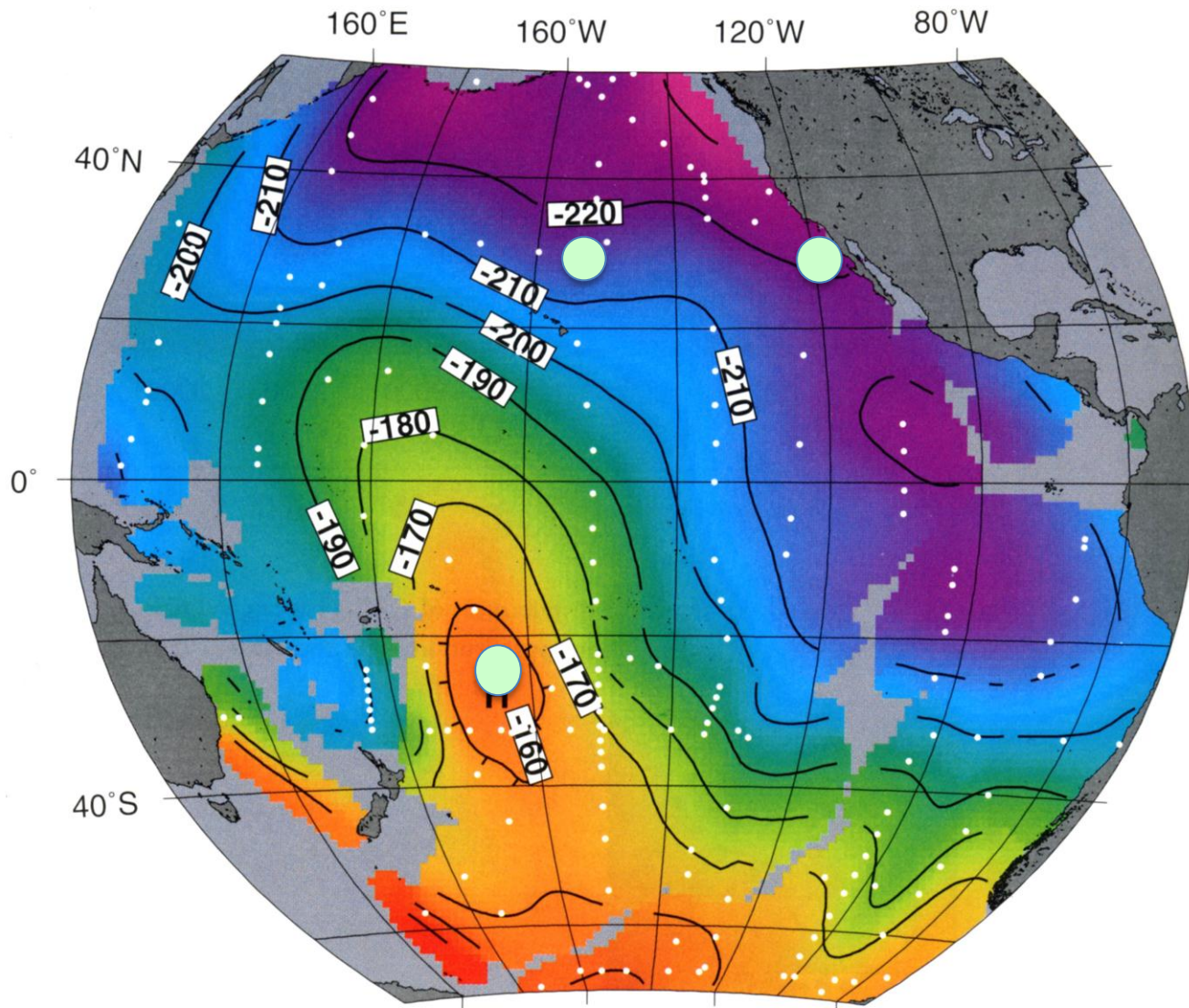


Talley (2007) WOCE Pacific Ocean Atlas

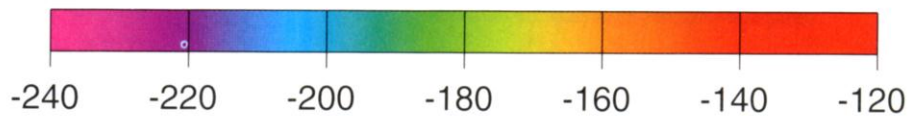
Delta Radiocarbon ($\delta^{14}\text{C}$) section in the central Pacific Ocean



Talley (2007) WOCE Pacific Ocean Atlas



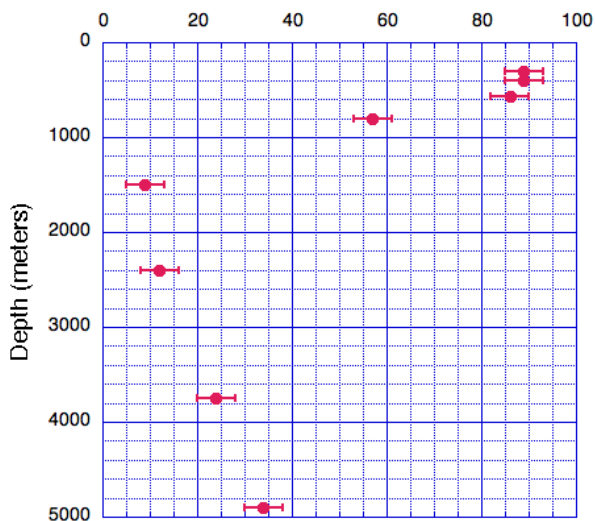
Near Bottom Values $\Delta^{14}\text{C}\text{‰}$



Ar-39 and C-14 Profiles in the Pacific Ocean

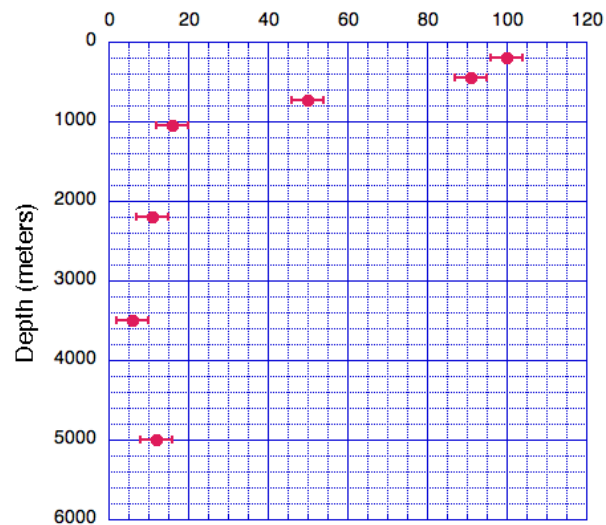
Tahiti

Ar-39 (% modern)



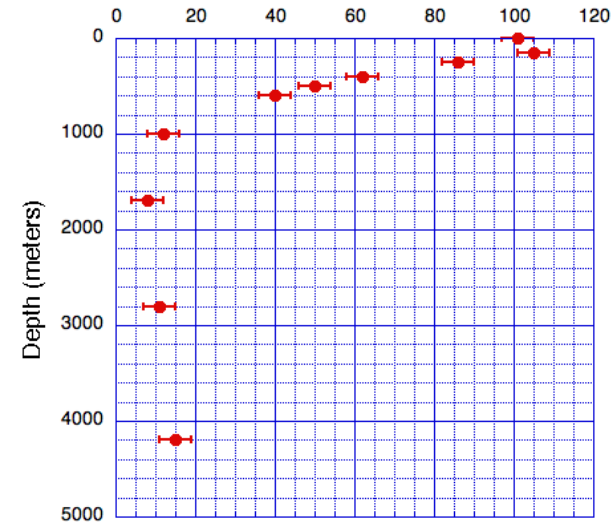
Hawaii

Ar-39 (% modern)



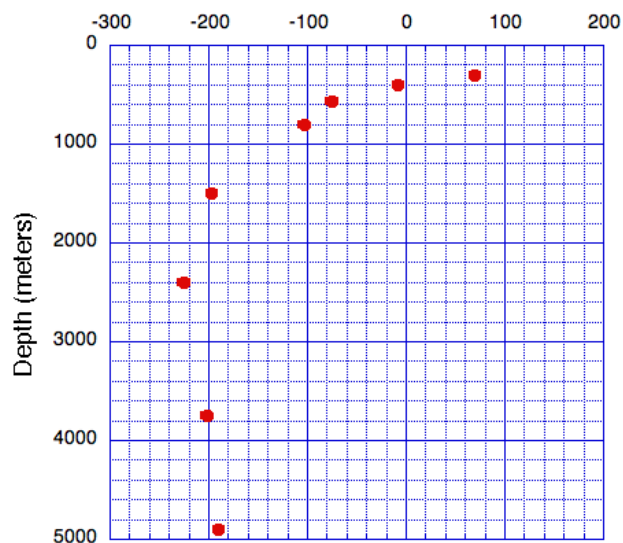
Geosecs 347

Ar-39 (% modern)



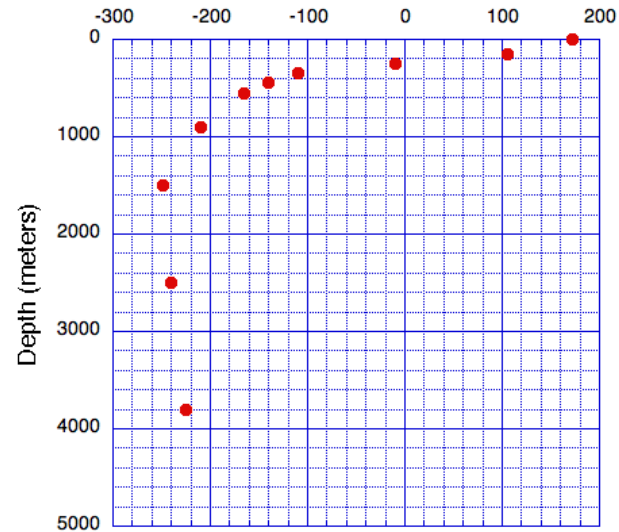
Tahiti

Delta C-14 (o/oo)



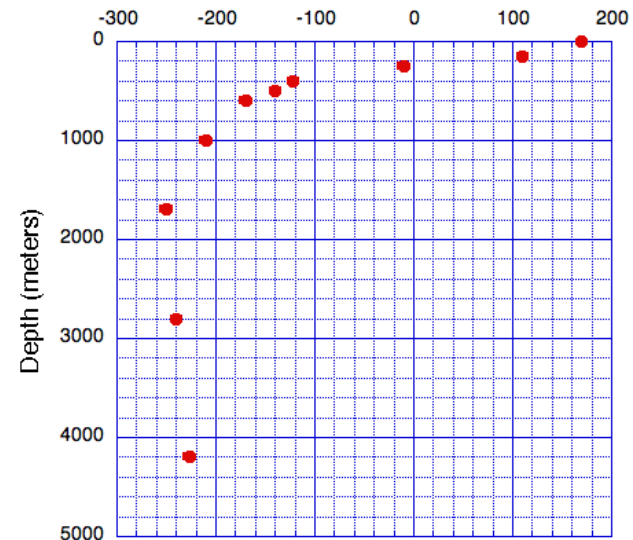
Hawaii

Delta C-14 (o/oo)



Geosecs 347

Delta C-14 (o/oo)



Data replotted from Rodriguez (1993) Ph.D. Thesis, University of Bern. See previous slide for locations.

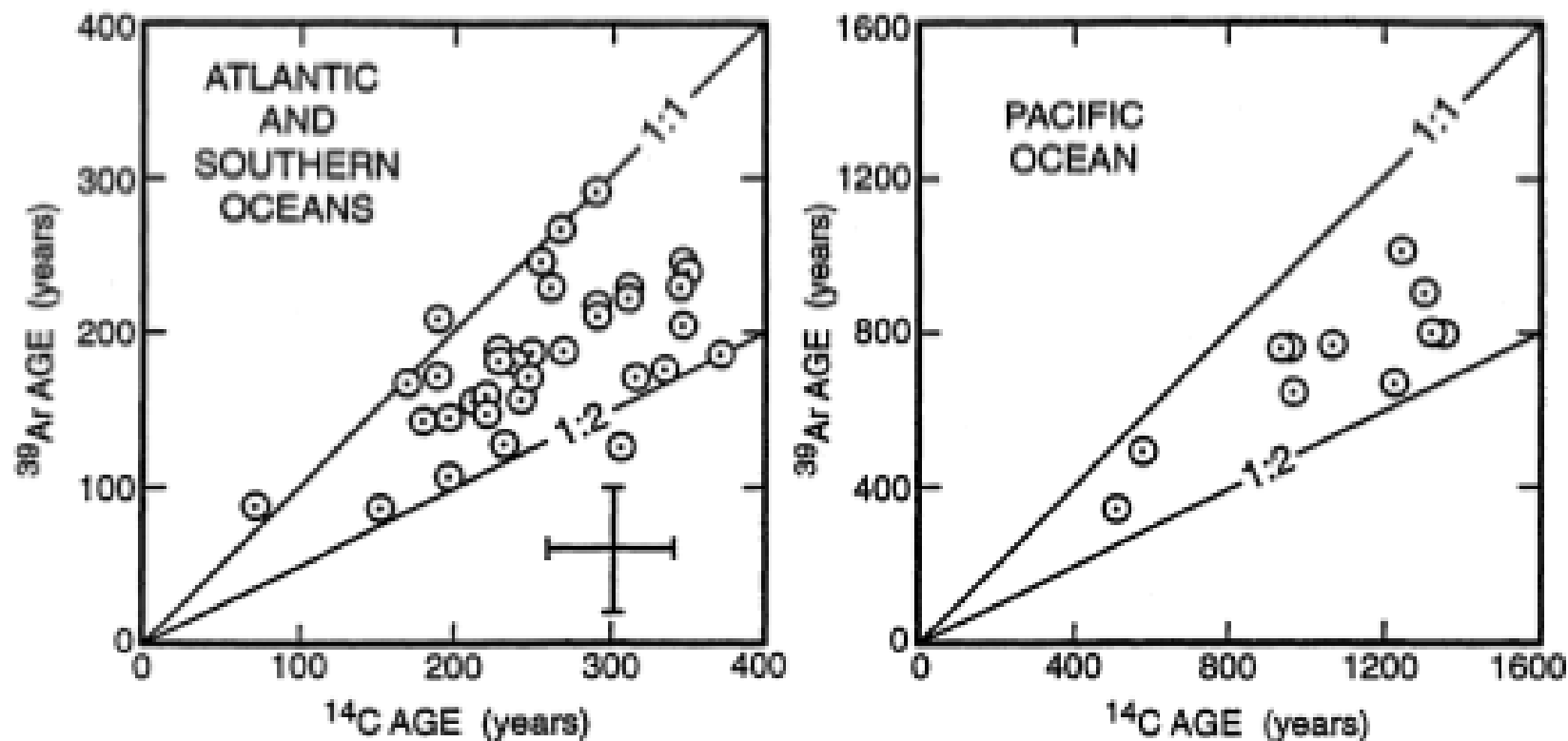


Fig. 1. Plots of ^{39}Ar age versus ^{14}C age for water samples from the Atlantic and Southern Oceans on the left and from the Pacific on the right. The ^{39}Ar ages are calculated assuming the original ^{39}Ar to Ar ratio is 0.85, the atmospheric value. The ^{14}C ages are calculated as outlined in the text. W.S. Broecker, T.-H. Peng / Nucl. Instr. and Meth. in Phys. Res. B 172 (2000) 473-478

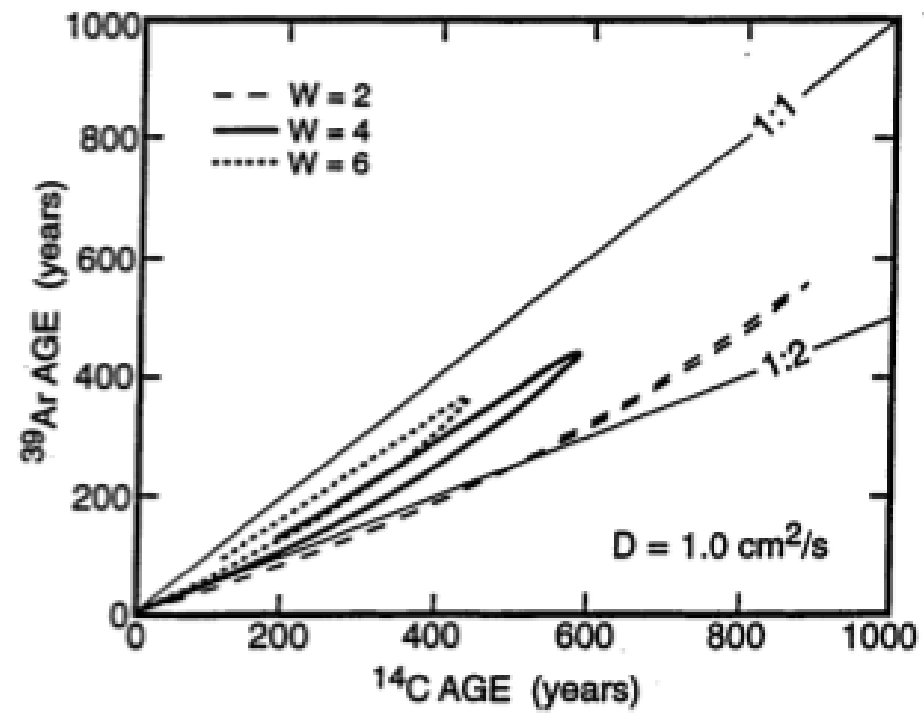
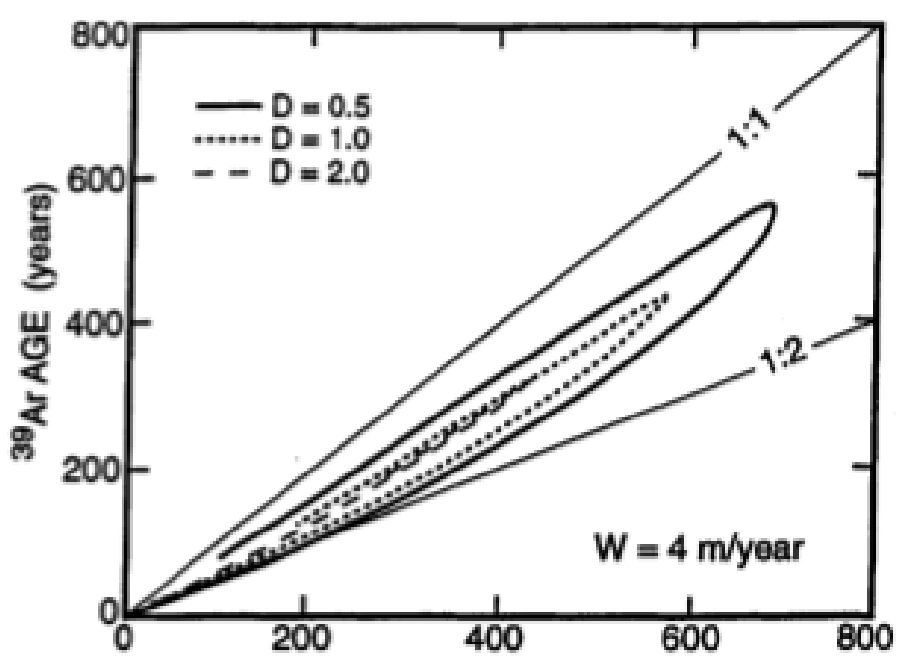


Fig. 2. Relationship between ^{39}Ar and ^{14}C ages for the simple one-dimensional upwelling diffusion model described in the text. As can be seen, the ^{39}Ar ages are younger than the ^{14}C ages. Further, for an upwelling velocity of 4 m/yr, the envelope follows the median slope for the data in Fig. 1. W.S. Broecker, T.-H. Peng / Nucl. Instr. and Meth. in Phys. Res. B 172 (2000) 473-478

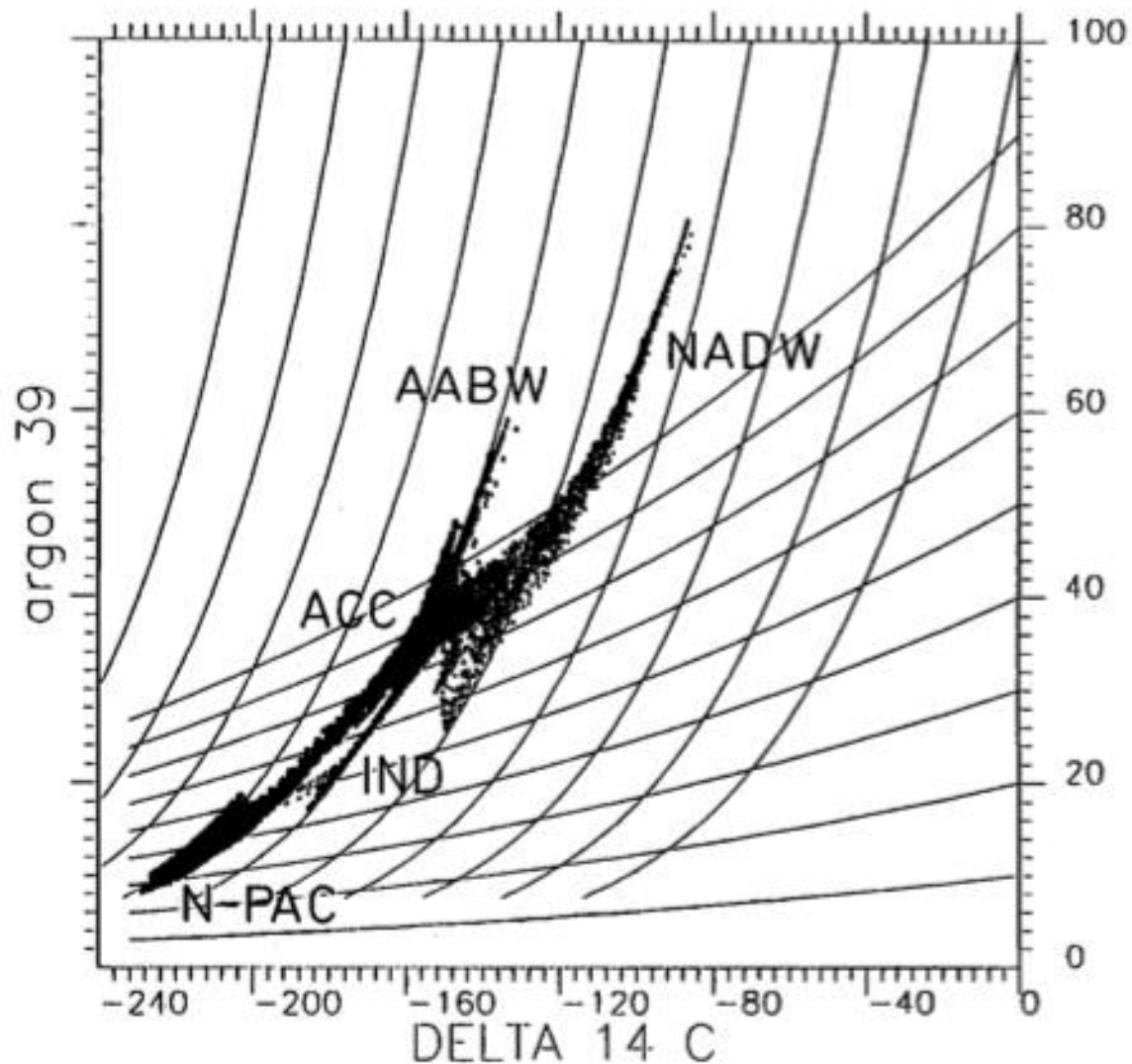


Fig. 13. Scatter of Argon 39 versus $\Delta^{14}\text{C}$ in the deep ocean below one km. The lines with steep slope indicate the theoretical advective aging for source waters with different radiocarbon content. The lines with flat slope indicate the same for exclusive diffusion. Maier-Reimer (1993)

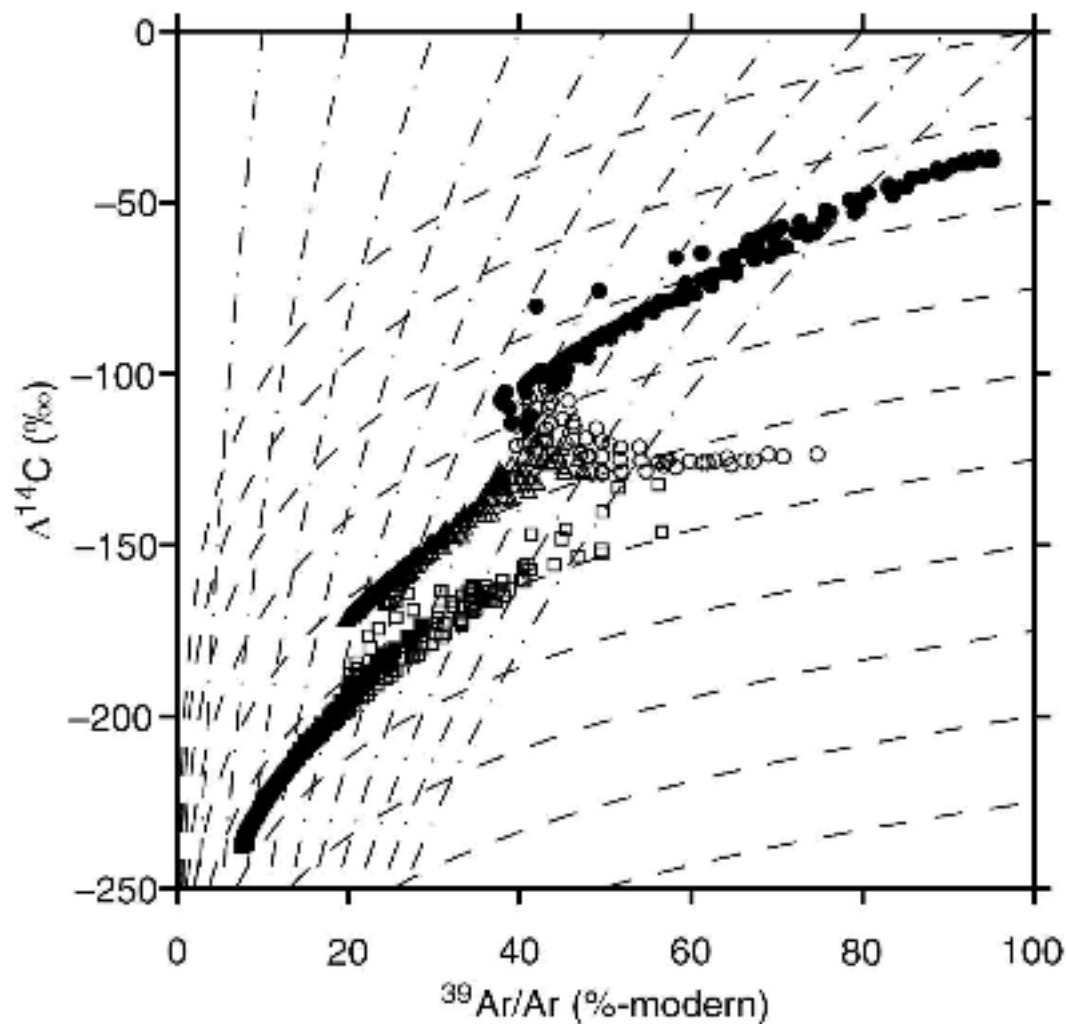


FIG. 13. Simulated $\Delta^{14}\text{C}$ vs $^{39}\text{Ar}/\text{Ar}$ values for all boxes at a depth of around 2000 m for the Atlantic (circles), Pacific (squares), and Indian (triangles) Oceans. Filled symbols are for regions north of 33.7°S . The dashed lines show trajectories in $\Delta^{14}\text{C}$ - $^{39}\text{Ar}/\text{Ar}$ space for pure advective transport; the dash-dotted lines are for pure diffusive transport (Maier-Reimer 1993).

Muller et al. (2006)

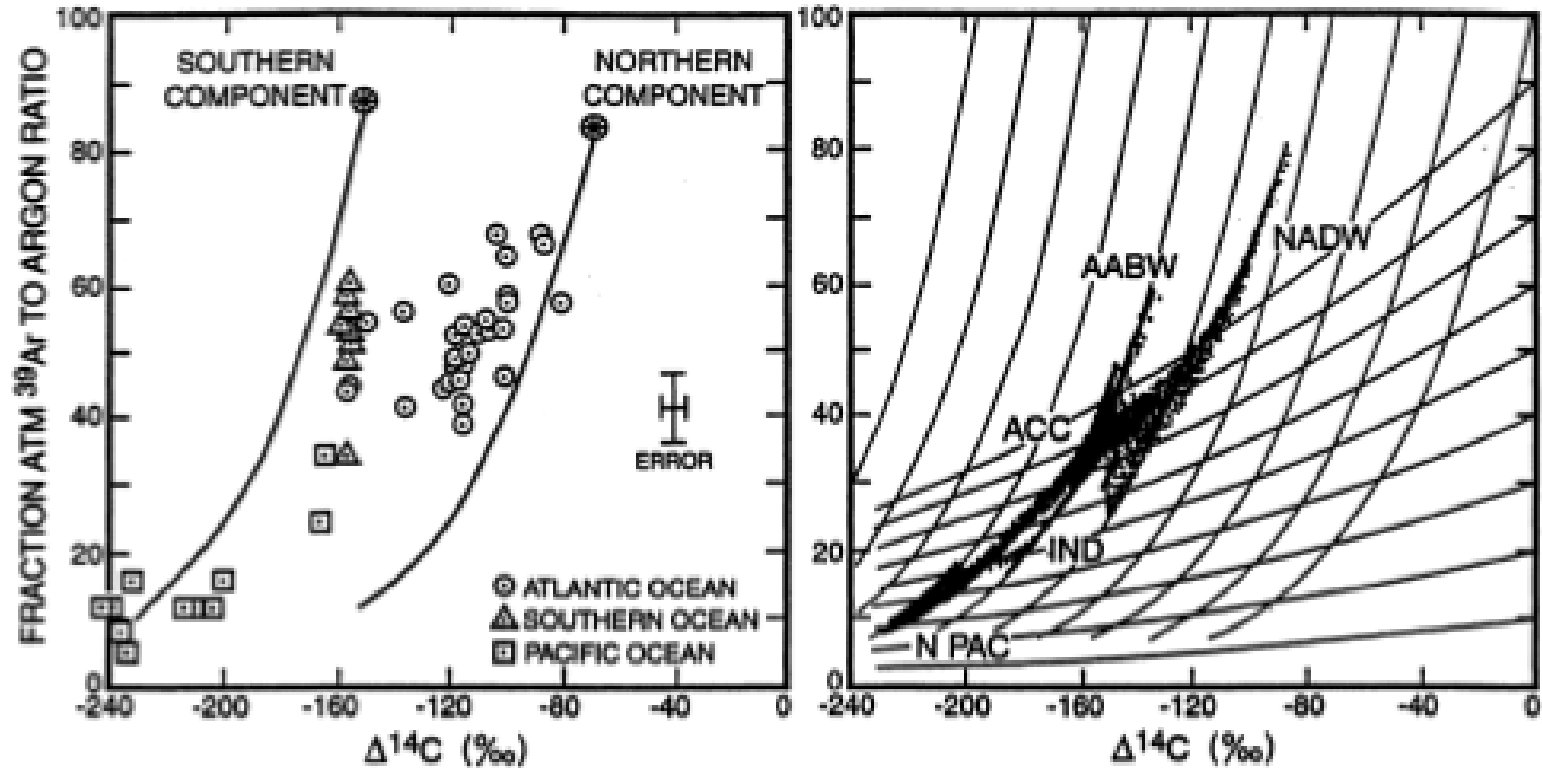
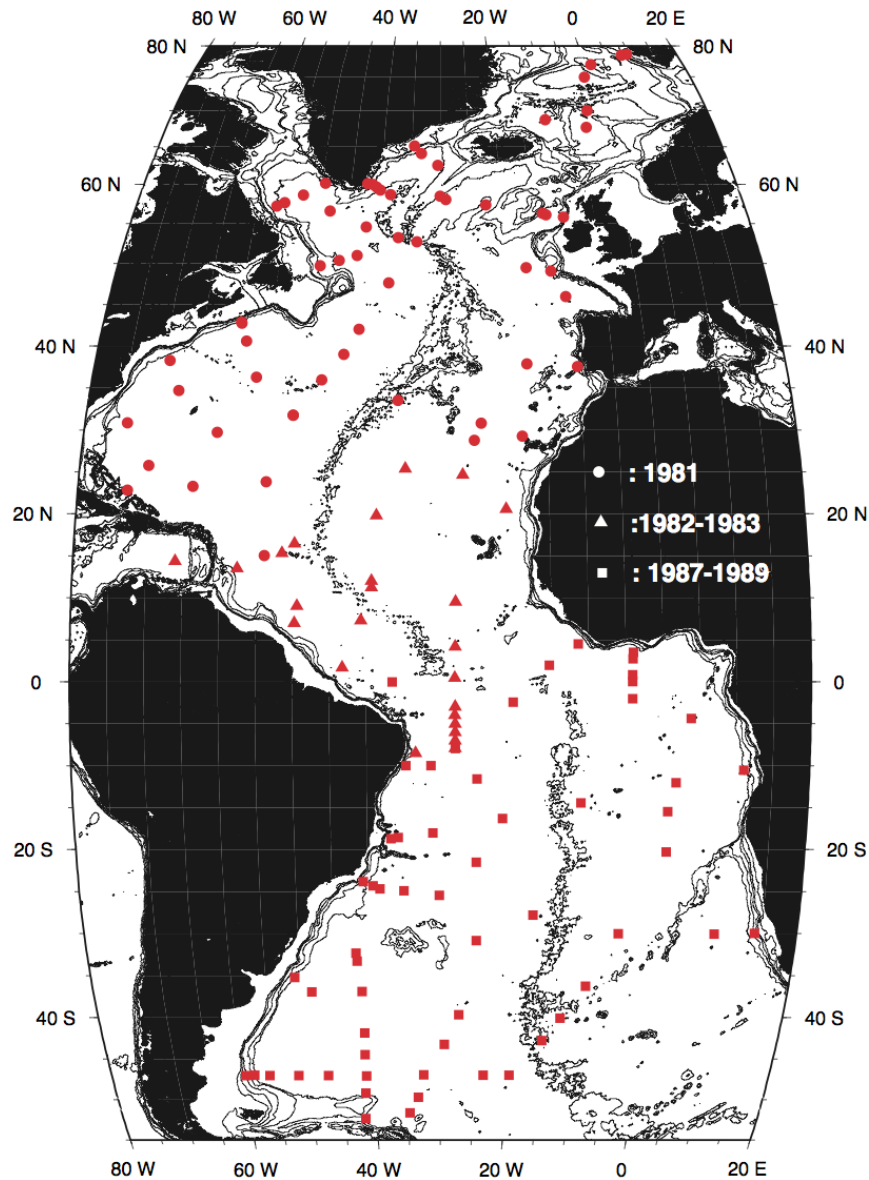
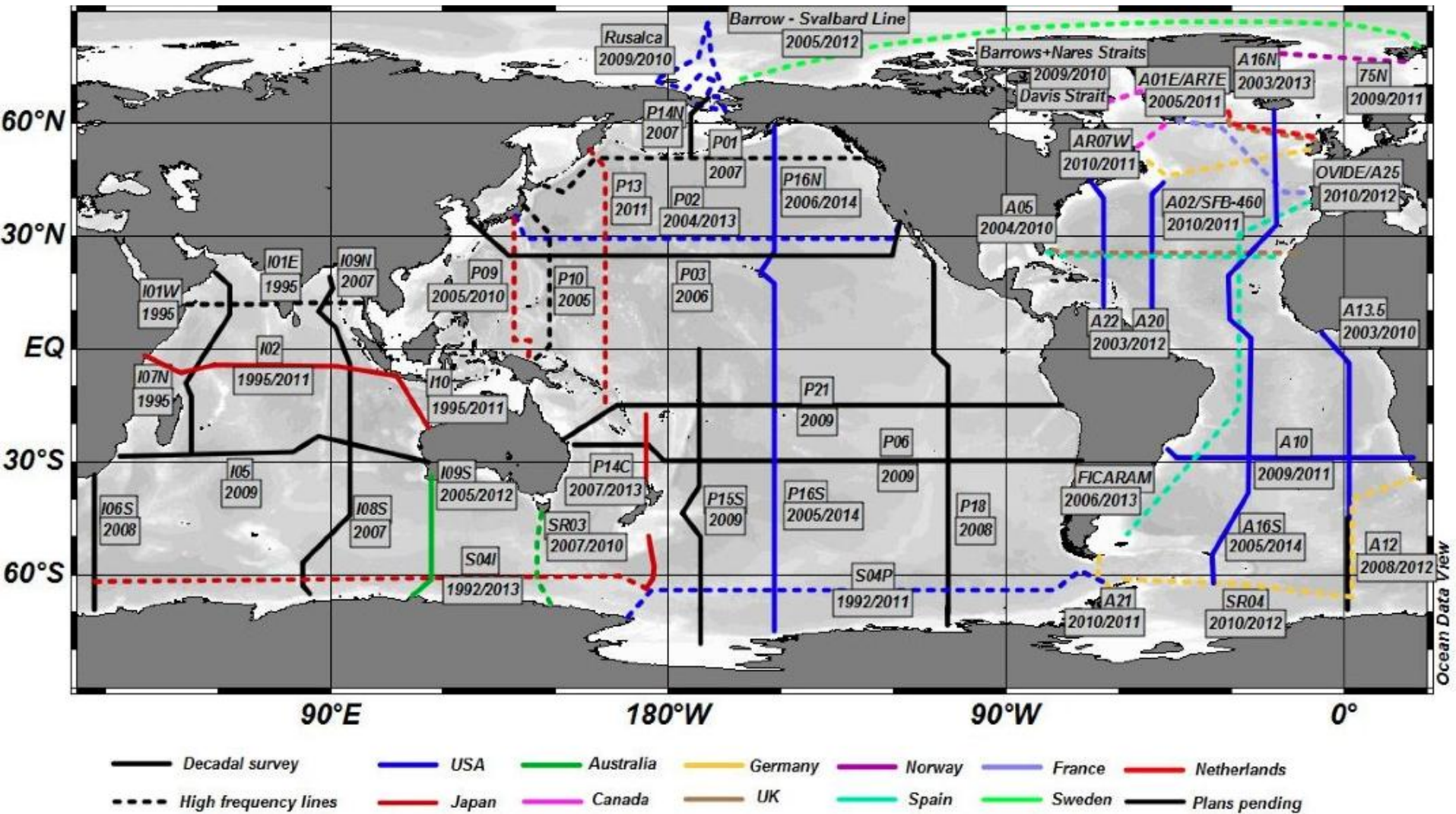


Fig. 3. Comparison between the measurements (left) and the output of the Hamburg ocean model (right). In both, the trends expected for radiodecay alone are shown. For the Hamburg ocean model [12], the set of lines with the lower slope reflect the impact of diffusion. The two trend lines shown in the left-hand panel portray the influence of radiodecay on deep water formed in the northern Atlantic and Southern Ocean, respectively. W.S. Broecker, T.-H. Peng / Nucl. Instr. and Meth. in Phys. Res. B 172 (2000) 473-478

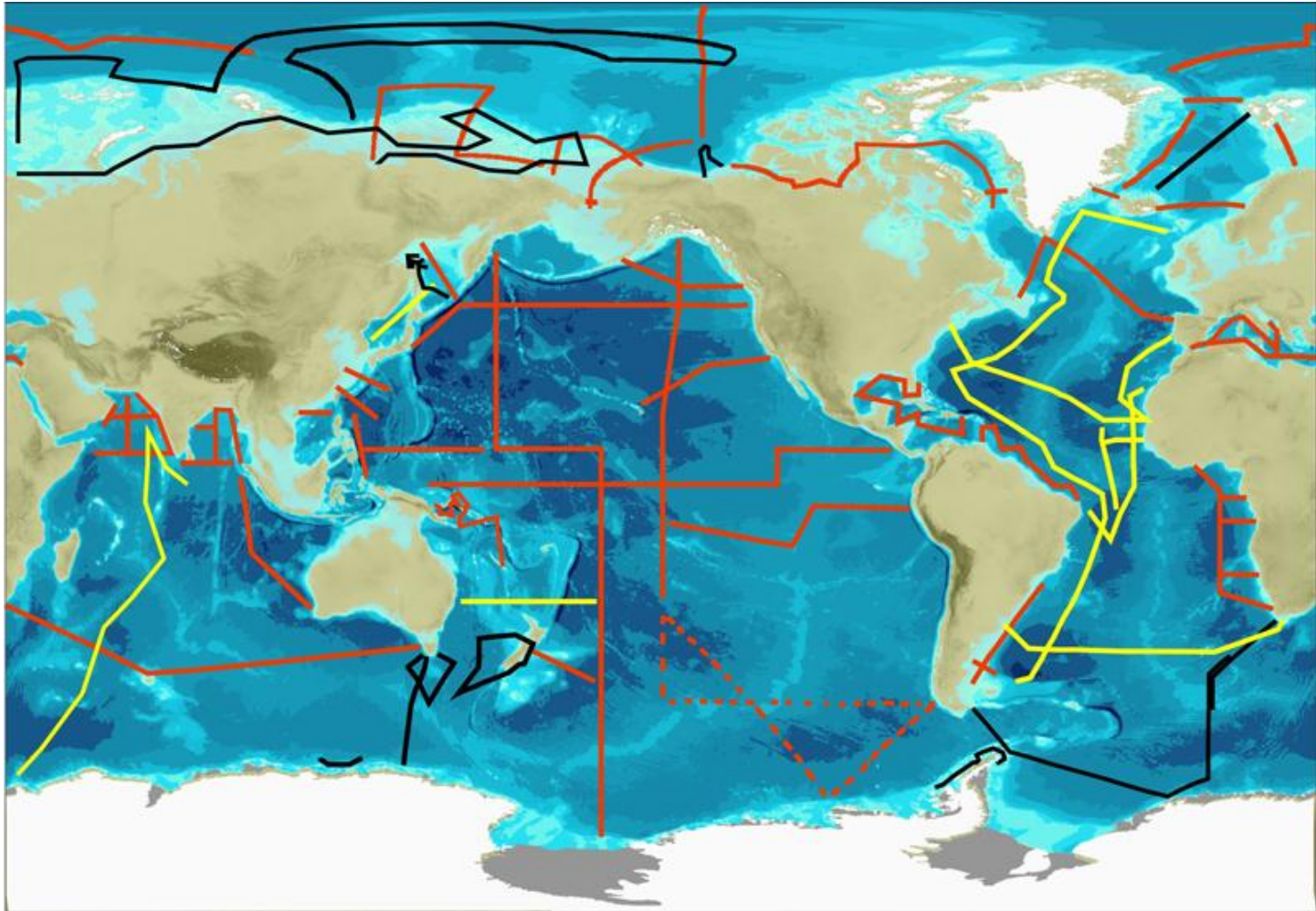


Locations of oceanographic stations where large volume (250 liters) samples were collected for measurement of C-14 and Kr-85. Either the argon fractions or the entire extracted gas samples have been archived at Lamont-Doherty Earth Observatory.

CLIVAR Repeat Hydrography Cruise Tracks



GEOTRACES Sections



Red: Planned sections

Yellow: Completed Sections

Black: Sections completed as part of IPY